

# Structural stability of $\text{TiO}_2$ at high pressure in density-functional theory based calculations

Xiang Wu<sup>1,2,3</sup>, Eva Holbig<sup>1</sup> and Gerd Steinle-Neumann<sup>1</sup>

<sup>1</sup> Bayerisches Geoinstitut, Universität Bayreuth, Bayreuth D-95440, Germany

<sup>2</sup> Key Laboratory of Orogenic Belts and Crustal Evolution, MOE and School of Earth and Space Sciences, Peking University, Beijing 100871, People's Republic of China

E-mail: [xiang.wu@pku.edu.cn](mailto:xiang.wu@pku.edu.cn)

Received 5 May 2010, in final form 30 May 2010

Published 28 June 2010

Online at [stacks.iop.org/JPhysCM/22/295501](http://stacks.iop.org/JPhysCM/22/295501)

## Abstract

A new study on the pressure-induced phase transitions of  $\text{TiO}_2$  has been performed using all-electron density-functional theory based computations with the projector augmented wave and the linearized augmented plane wave methods considering five experimentally observed structures. The static results yield a picture that is consistent with experiments, i.e., phase transitions with pressure are predicted as rutile  $\rightarrow$  monoclinic baddeleyite (MI)  $\rightarrow$  orthorhombic I (OI)  $\rightarrow$  cotunnite (OII) on compression, and OII  $\rightarrow$  OI  $\rightarrow$  MI  $\rightarrow$  columbite ( $\text{TiO}_2$ II) on decompression. The elasticities of these five polymorphs are compared. Except for the baddeleyite structure, which is considerably softer than the other polymorphs, all phases show a zero pressure bulk modulus in the range of 200–240 GPa, consistent with compression results and the single crystal elastic constant; on the basis of these results we can say that the cotunnite phase is not a superhard  $\text{TiO}_2$  polymorph as has been suggested previously. We further find that the rutile and columbite structures are energetically very similar, with the columbite structure favored slightly. All polymorphs are predicted as insulating with comparable band gaps ( $\sim$ 1.7–2.3 eV). Crystal field splitting for the Ti 3d electronic states leads to two distinct conduction bands in rutile and  $\text{TiO}_2$ II for energies smaller than 8 eV, while there is a single conduction band for the other high pressure structures.

(Some figures in this article are in colour only in the electronic version)

## 1. Introduction

Titanium dioxide ( $\text{TiO}_2$ ) is a very important technological material, which is widely used as a white pigment and opacifier due to its brightness and very high refractive index ( $n = 2.7$ ) [1], and also applied in photocatalysts and electrochemical dye solar cells due to its wide bandgap ( $E_g = 3.0$  eV) [2]. The possibility to quench high pressure forms of  $\text{TiO}_2$  to ambient conditions with different properties is potentially of great importance for technological applications [3]. As rutile is isostructural to the high pressure form of  $\text{SiO}_2$ , stishovite, it is also of considerable interest for studies of mineral stability at high pressure and relevant for the structure of the Earth's interior, especially when investigating post-stishovite phases for  $\text{SiO}_2$  rich compositions such as basalts [4]. As a

consequence, the high pressure structural behavior of  $\text{TiO}_2$  is a classical subject in material and mineral sciences.

In natural samples at ambient conditions,  $\text{TiO}_2$  often occurs in the rutile (space group  $P4_2/mnm$  and  $Z = 2$ ), anatase ( $I4/amd$  and  $Z = 4$ ) and brookite ( $Pbca$  and  $Z = 8$ ) structures. Calorimetric measurements show that among them rutile has the lowest enthalpy of formation [5–8]. To date rich high pressure polymorphism of  $\text{TiO}_2$  has been observed experimentally: columbite (referred to as  $\text{TiO}_2$ II,  $Pbcn$  and  $Z = 4$ ), baddeleyite (MI,  $P2_1/c$  and  $Z = 4$ ), orthorhombic I (OI,  $Pbca$  and  $Z = 8$ ), and cotunnite (OII,  $Pnma$  and  $Z = 4$ ) respectively [9–20]. The observation and potential nature of cubic  $\text{TiO}_2$  (in the fluorite or pyrite structure) as the post-OI phase is still controversial [3, 21, 22].

When compressing rutile, it transforms to MI at  $\approx$ 12 GPa [10–20], and to OI at 25–30 GPa by laser

<sup>3</sup> Author to whom any correspondence should be addressed.

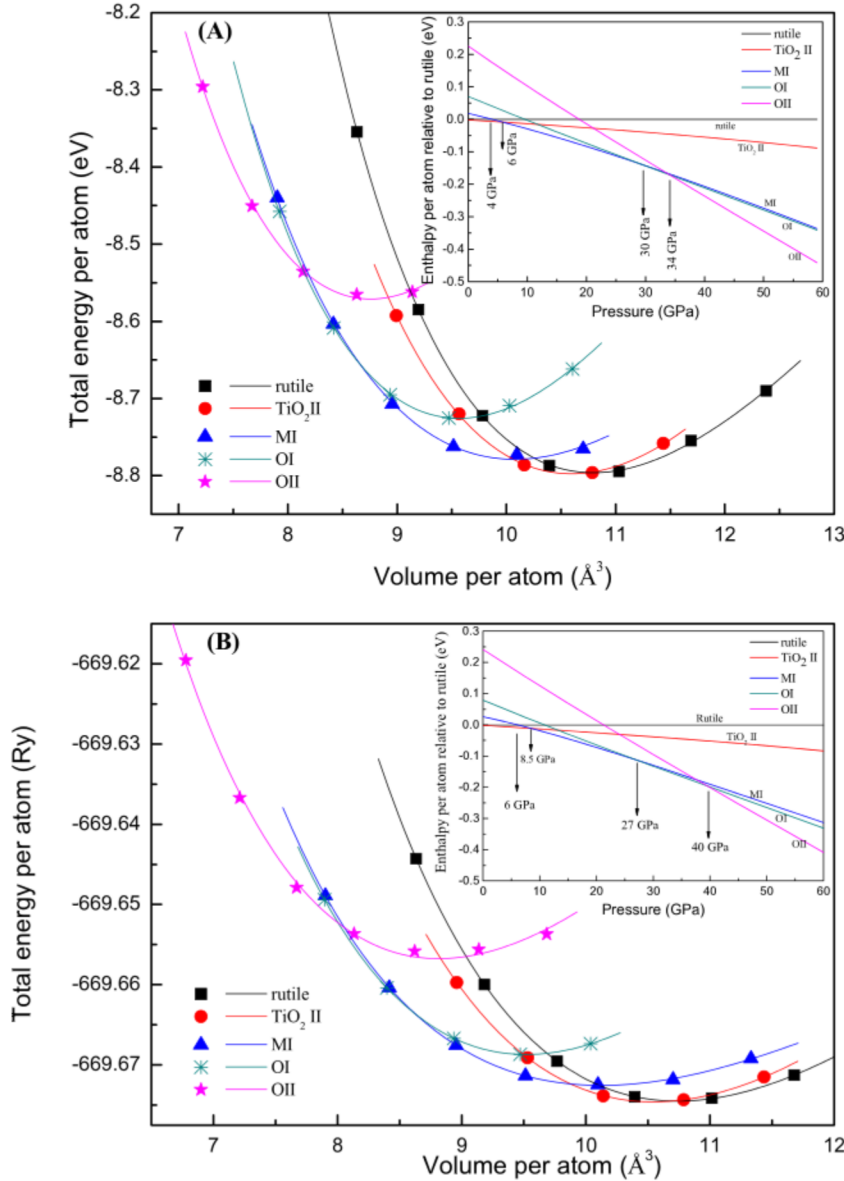


**Figure 1.** Total energy versus volume curves for the rutile,  $\text{TiO}_2\text{II}$ , MI, OI, and OII phases of  $\text{TiO}_2$  and calculated enthalpies versus pressure for all phases (inset). (A) for PAW-GGA; (B) for LAPW-GGA.

heating, then to OII at 48 GPa [16, 19, 20]. On decompression, phase transitions occur from MI to  $\text{TiO}_2\text{II}$  below 10 GPa [13–16, 19, 20], and  $\text{TiO}_2\text{II}$  is the only phase quenched to ambient conditions [19, 20]. As far as we know,  $\text{TiO}_2\text{II}$  has never been observed *in situ* in x-ray diffraction experiments for rutile as starting material on compression at room temperature. In Raman studies, however rutile has been proposed to transform directly to  $\text{TiO}_2\text{II}$  [23–25].

There is considerable discrepancy between different computational studies on  $\text{TiO}_2$  phase stability at high pressure using electronic structure methods. A general agreement is that the  $\text{TiO}_2\text{II}$  phase is stable between rutile and the MI structure [16, 18, 26–28], and about the initial phase transition sequence both within the local density (LDA) [26] and generalized gradient (GGA) [28] approximations to the exchange and correlations potential: rutile  $\rightarrow$   $\text{TiO}_2\text{II}$   $\rightarrow$  MI. Sasaki [28] further predicted that the OI structure

has higher energy than MI, up to at least 80 GPa, and was unlikely to be the post-MI phase. However, competing LDA full-potential linear-muffin-tin-orbital (FP-LMTO) simulations predicted the OI structure as the post-MI phase, with an extended phase transition sequence: rutile  $\rightarrow$   $\text{TiO}_2\text{II} \rightarrow$  MI  $\rightarrow$  OI  $\rightarrow$  OII [16, 18], also confirmed by LDA-linearized combination of atomic orbitals (LCAO) computations (not considering the OI phase) [27]. All cubic structures considered as the post-OI phase are predicted to be unstable at high pressure in computations [16, 18, 27, 28].

Some high pressure phases of  $\text{TiO}_2$  (cottonite OII and potential cubic phases) have been proposed to be superhard materials [17, 21]. For the OII phase experiments have reported an extrapolated  $B_0 = 431$  GPa [17, 18], a value that has been supported by Hartree–Fock computations that predicted  $B_0 = 380$  GPa [27]. In more recent work it has been pointed out that the approximation to the exchange and correlation

**Table 1.** Equation of state parameters for five polymorphs of  $\text{TiO}_2$ .  $V_0$ ,  $B_0$ , and  $B'_0$  are the volume per formula unit at zero pressure, the bulk modulus at  $V_0$ , and its pressure derivative, respectively.

Phase	$V_0$ ( $\text{\AA}^3$ )	$B_0$ (GPa)	$B'_0$	Method and reference
Rutile	32.4	200	5.6	PAW-GGA <sup>a</sup>
	32.2	203	5.2	LAPW-GGA <sup>a</sup>
	30.47	250	4.0	LDA [20]
	32.18	216	4.0	GGA [20]
	31.89	215	5.35	GGA [21]
	31.7	224	5.6	B3LYP [21]
	32.9	200	5.75	GGA [30]
	31.65	235	4.0	GGA [37]
	31.2	210(10)	6.6(7)	Exp. [14]
	31.20	235	4	Exp. [20]
	—	211(7)	6.84	Exp. [38]
	31.22	211(1)	6.76	Exp. [39]
$\text{TiO}_2\text{II}$	31.8	208	4.0	PAW-GGA <sup>a</sup>
	31.6	206	4.1	LAPW-GGA <sup>a</sup>
	29.97	212	4	LDA [20]
	31.75	188	4	GGA [20]
	31.3	250(23)	2.6(7)	GGA [21]
	31.2	257(12)	2.6(4)	B3LYP [21]
	30.7	264(10)		LCAO-HF [27]
	30.96	257	1.99	GGA [28]
	30.6	258(8)	4.05(25)	Exp. [14]
	30.6	258(8)	4.1(3)	Exp. [15]
	30.56	206	4	Exp. [19]
	30.53	253	4	Exp. [20]
MI	30.3	145	4.0	PAW-GGA <sup>a</sup>
	30.3	125	5.4	LAPW-GGA <sup>a</sup>
	28.01	190	4	LDA [20]
	29.96	157	4	GGA [20]
		300(10)		LCAO-HF [27]
	29.9	148	4.21	GGA [28]
	28.06	290(20)	4(fixed)	Exp. [14]
	28.05	290(10)	4(fixed)	Exp. [15]
	28.84	175	4	Exp. [19]
	28.06	298	4	Exp. [20]
OI	28.7	220	4.1	PAW-GGA <sup>a</sup>
	28.6	223	3.9	LAPW-GGA <sup>a</sup>
	27.02	236	4	LDA [20]
	28.71	209	4	GGA [20]
	28.3	272(9)	3.38(19)	B3LYP [21]
	29.27	214	2.33	GGA [28]
	27.3	318 ± 3	4.0	Exp. [16]
	27.96	222	4	Exp. [19]
	27.54	314	4	Exp. [20]
OII	26.3	235	4.0	PAW-GGA <sup>a</sup>
	26.5	220	4.0	LAPW-GGA <sup>a</sup>
	24.44	300	4	LDA [20]
	25.97	261	4	GGA [20]
	—	380(10)		LCAO-HF [27]
	23.8	341	3.85	LDA [29]
	25.4	281	4.8	GGA [29]
	27.15	272	4.09	GGA [30]
	26.3	431(10)	1.35(10)	Exp. [17, 18]
	25.10	306	4	Exp. [19]
	25.28	312	4	Exp. [20]

<sup>a</sup> This study.

potential (LDA versus GGA) results in a large difference of  $B_0$ , with LDA yielding values in excess [27, 29] and GGA below 300 GPa [20, 29, 30], a value much lower than experimental data. Also, two recent experimental re-investigations of OII-

$\text{TiO}_2$  resulted in data that were in discrepancy with the previous measurements, and yielded a lower  $B_0$  (306 GPa [19] and 312 GPa [20]) when  $B'_0$  was fixed as 4.0.

This discussion clearly illustrates why additional careful electronic structure computations are required to clarify some of the discrepancies reported in the literature. Here we perform computations using two highly accurate all-electron methods within DFT and GGA to explore the high pressure phase stability and equations-of-state of  $\text{TiO}_2$  polymorphs. Computations of single crystal elastic constants allow us to cross-check the bulk modulus obtained from fitting energy–volume relations using finite strain theory.

## 2. Methods

Calculations performed here are based on DFT with GGA, as implemented in the VASP [31] and WIEN2K [32] packages. In VASP we used the projector augmented wave (PAW) method [33] within the GGA formulation by Perdew *et al* [34] through the potentials supplied with the VASP package. We set the kinetic energy cut-off for plane wave expansion to 700 eV in order to obtain fully converged results. For Brillouin zone sampling, we used the Monkhorst–Pack scheme with  $4 \times 4 \times 6$   $k$ -points for  $\text{TiO}_2$  rutile,  $4 \times 4 \times 4$  for  $\text{TiO}_2\text{II}$  and MI,  $2 \times 4 \times 4$  for OI, and  $2 \times 4 \times 2$  for OII. Computations were performed for a number of different volumes for each crystalline system. Energy–volume results were fitted with a third-order equation of state (Birch–Murnaghan EoS) [35]. Single crystal elastic constants were computed from stress–strain relations [36], straining the lattice and computing the resulting elastic constant tensor through changes in the stress tensor ( $\underline{\sigma}$ ) with respect to applied strain ( $\underline{\epsilon}$ ). Positive and negative strains of magnitude 1% were used in order to accurately determine the stresses in the appropriate limit of zero strain.

In addition, we performed calculations with the linearized augmented plane wave + local orbitals (LAPW + lo) method. As for the PAW computations we treated effects of exchange and correlation by GGA [34]. The muffin-tin radii of Ti and O were kept constant for the different structures as 1.6 and 1.8 Bohr, respectively. The size of the basis is set by  $R_{\text{MT}} * K_{\text{MAX}} = 7.0$ , and reciprocal space sampling was chosen with 1000  $k$ -points in the full Brillouin zone. Structure and atomic positions were fully optimized again within the LAPW computations, except for the monoclinic phase (MI) where the cell geometry was fixed to that from the PAW computations (but positions were optimized in the LAPW computations). The LAPW  $E$ – $V$  results were also fitted with a third-order Birch–Murnaghan EoS [35].

## 3. Results and discussion

### 3.1. Phase stability and equation of state

The total energies, calculated as a function of the volume for five phases, are compared in figure 1(A) (PAW) and (B) (LAPW); solid lines are the finite strain EoS fit to the results. The corresponding parameters for the EoS are listed in table 1,

**Table 2.** The sequence of phase transitions and corresponding phase transition pressures (units: GPa).

Phase	P.trans.	Phase	P.trans.	Phase	P.trans.	Phase	Method
On compression							
rutile →		MI →		OI →		OII	
4		30		34			PAW–GGA <sup>a</sup>
6		27		40			LAPW–GGA <sup>a</sup>
12							Exp. [12]
12							Exp. [13]
12		30		48			Exp. [16]
12		23–29		37.4			Exp. [19]
12		25		49			Exp. [20]
On decompression							
OII →		OI →		MI →		TiO <sub>2</sub> II	
	34		30		6		PAW–GGA <sup>a</sup>
	40		27		8.5		LAPW–GGA <sup>a</sup>
					9.7		Exp. [12]
					7		Exp. [13]
					7		Exp. [15]
	38		20		7		Exp. [16]
			20		8		Exp. [20]

<sup>a</sup> This study.**Table 3.** Single crystal elastic constants of TiO<sub>2</sub> polymorphs at zero pressure and bounds on their bulk and shear moduli computed from the elastic constants (units: GPa).

	Rutile			TiO <sub>2</sub> II		MI		OI		OII	
	GGA PAW–GGA <sup>a</sup> [37]	GGA PAW–GGA <sup>a</sup> [30]	Exp. [39–41]	PAW–GGA <sup>a</sup>	SIESTA–GGA [29]	SIESTA–LDA [29]					
C <sub>11</sub>	271	278	276	267–271	296	276	355	478	619	688	
C <sub>12</sub>	147	153	154	175–181	160	75	132	165	218	258	
C <sub>13</sub>	148	149	152	147–150	160	40	118	191	178	240	
C <sub>15</sub>					68						
C <sub>22</sub>					286	293	449	291	350	510	
C <sub>23</sub>					139	57	117	85	82	253	
C <sub>25</sub>					25						
C <sub>33</sub>	451	479	483	479–484	364	235	359	279	282	649	
C <sub>35</sub>					17						
C <sub>44</sub>	109	115	113	123–124	82	51	82	58	52	129	
C <sub>46</sub>					4						
C <sub>55</sub>					117	119	70	38	43	133	
C <sub>66</sub>	214	214	211	189–195	60	110	132	129	219	204	
B <sub>R</sub>	199		205	208–211	205	122	208	185	196	367	
B <sub>V</sub>	209		217	218–220	207	128	210	214	245	372	
B <sub>0</sub>	204	204	211	213–216	206	125	209	200	221	369	
G <sub>R</sub>	104		107	95–99	79	86	101	69	77	158	
G <sub>V</sub>	123		126	123–125	84	98	110	85	114	166	
G <sub>0</sub>	114	118	116	109–112	82	92	106	77	96	162	

<sup>a</sup> This study.

which includes the available experimental and theoretical data for comparison [14–21, 27–29, 37–39]. The results from PAW–GGA and LAPW–GGA methods are virtually identical. The equilibrium volumes ( $V_0$ ) are overestimated by 4%, compared with those of experimental results for all phases [14–20, 38, 39] which is typical for GGA computations and consistent with previous computations on TiO<sub>2</sub> [20, 21, 27–30]. The zero pressure bulk modulus for rutile (200–203 GPa) is in good agreement with the experimental result (211 GPa) [14, 38, 39] and the B3LYP and GGA results (190–224 GPa) [20, 21, 30]. Except for MI, which shows a significantly lower  $B_0$ , the bulk moduli for the TiO<sub>2</sub> phases are very similar, in the range of

200–240 GPa. Especially for the orthorhombic phase (OII) this is considerably lower than the extrapolation from the experimental data (table 1) [18–21]. One of the reasons for this discrepancy is due to the trade-off between  $V_0$ ,  $B_0$  and its pressure derivative ( $B'_0$ ) in the EoS fitting procedure, especially for MI and OII where only high pressure data are available. In [16] and [17], the  $B'_0$  of cotunnite TiO<sub>2</sub> (1.35) is extremely small, resulting in an overestimate of  $B_0$ . Constraining  $B'_0 = 4.0$  a different set of experiments did yield a  $B_0 = 306$ –312 GPa [20, 21], still considerably larger than the GGA computations performed here and in their own work [21]. Our fit results are independently confirmed from the single crystal

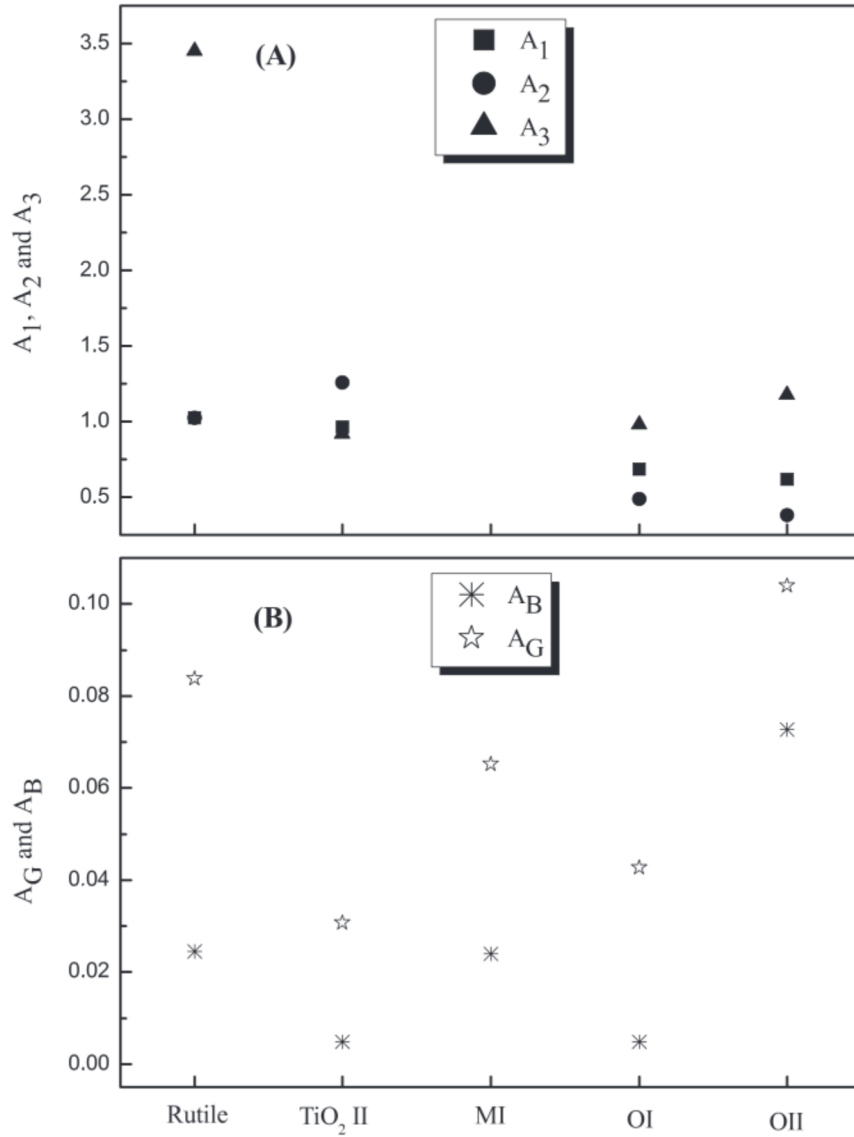


**Figure 2.** The Zener ratios ( $A_1$ ,  $A_2$ , and  $A_3$ ) and anisotropy factors ( $A_B$  and  $A_G$ ) for five polymorphs of  $\text{TiO}_2$ .

elastic constant computations (discussed in more detail below) that yield a Voigt–Reuss–Hill average for  $B_0$  of 200 GPa at the zero pressure volume (table 3).

From our computations we find the rutile and  $\text{TiO}_2$  II phase energetically very similar (with  $\text{TiO}_2$  II having slightly lower energy at low compression), and subsequent phase transitions under pressure occur to the MI, OI, and OII phases. Converting internal energies to enthalpies using the EoS (figure 1) and starting with rutile we predict a transition to the MI phase at  $\sim 5$  GPa, to OI at  $\sim 30$  GPa, and to OII at  $\sim 40$  GPa, in close agreement with experiments [12, 13, 15, 16, 19, 20] (table 2). On decompression the MI phase converts to  $\text{TiO}_2$  II at  $\sim 7$  GPa, never recovering the rutile structure, also in agreement with experiments that are unable to back-transform  $\text{TiO}_2$  to rutile under decompression [19, 20]. The small energetic difference between  $\text{TiO}_2$  II and rutile at  $V_0$  (+33 meV/f.u. in calorimetric measurements [5] and  $-4$  meV/f.u. in the computations) are most likely the reason for the absence of  $\text{TiO}_2$  II on compression, and rutile on decompression.

#### 4. Elasticity

The single crystal elastic constants of all five  $\text{TiO}_2$  polymorphs were computed at the theoretical equilibrium volumes ( $V_0$ , table 1) using a linear stress–strain relation based on generalized Hooke's law (table 3). The six independent single crystal elastic constants of the rutile phase are consistent with previous experimental [39–41] and theoretical results [30, 37] (table 3). In the rutile phase,  $C_{33}$  is larger than  $C_{11}$  as expected, because the  $c$  axis is parallel to the chains of edge-sharing  $\text{TiO}_6$  octahedra, resulting in greater stiffness. However, elastic constants of the OII phase are inconsistent between our results and previous computations using LDA and GGA implemented in the SIESTA software [29]. Especially the longitudinal elastic constants  $C_{11}$ ,  $C_{22}$  and  $C_{33}$  are affected. One of the reasons is that the zero pressure volume is  $26.3 \text{ \AA}^3$  per molecular formula in our calculations, but  $23.8 \text{ \AA}^3$  (LDA) or  $25.4 \text{ \AA}^3$  (GGA) in [29], i.e. at considerably lower volume (higher pressure) which should yield considerably

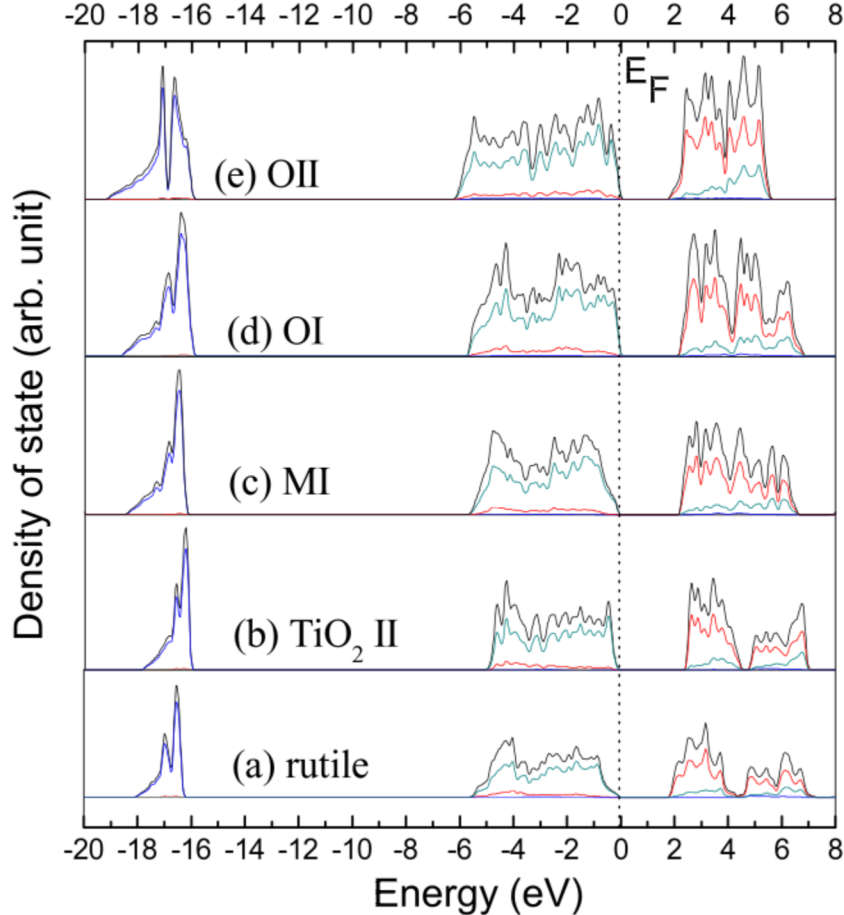


**Figure 3.** Electronic density of states (DOS) of the five  $\text{TiO}_2$  phases from LAPW–GGA computations at computational zero pressure volumes. The uppermost (black) curve shows the total DOS. For the conduction band ( $E > E_F$ ) the main contribution (red) stems from Ti 3d states, with a minor component from O 2p states (green). The upper valence band (near  $E_F$ ) of the DOS is dominated by O 2p states (green), the lower valence band O s electrons (blue).

stiffer elastic moduli. Further, the elasticity of OII– $\text{TiO}_2$  is sensitive to the treatment of the exchange–correlation energy, as illustrated by the previous results [29] that show very different values between LDA and GGA, e.g. for  $C_{33}$  a value of 649 GPa in LDA versus 282 GPa in GGA computations. In addition, using and averaging positive and negative strains is very important in order to obtain reliable results. In our case, a strain of magnitude 1% was used, while 2% was applied in [29], further away from the approximation of infinitesimal strain.

The bulk ( $B$ ) and shear ( $G$ ) moduli of the aggregate can be obtained from the single crystal elastic constants by the Voigt–Reuss–Hill approximation  $B = (B_V + B_R)/2$  and  $G = (G_V + G_R)/2$ , where V denotes the Voigt and R the Reuss average [42]. The values for the bulk moduli computed this way by use of the polycrystal software [43] are in good agreement with the  $E$ – $V$  EoS fitting (table 3), providing a cross-check with the compression results.

Single crystal anisotropy (except the monoclinic MI phase) can be described by three shear anisotropy factors (Zener ratios) [44]:  $A_1 = 4C_{44}/(C_{11} + C_{33} - 2C_{13})$  for the (100) shear plane,  $A_2 = 4C_{55}/(C_{22} + C_{33} - 2C_{23})$  for the (010) shear plane, and  $A_3 = 4C_{66}/(C_{11} + C_{22} - 2C_{12})$  for the (001) shear plane. A value of one indicates elastic isotropy,

and departure from unity corresponds to the degree of elastic anisotropy (figure 2(A)). In rutile, the (100) and (010) shear planes are nearly isotropic with  $A_1 = A_2 = 1.02$ , but with  $A_3 = 3.45$  a much larger shear anisotropy in the (001) plane exists. In the  $\text{TiO}_2$  II phase, the three Zener ratios are similar and close to one, indicating there is not much anisotropy. The orthorhombic phases OI and OII are more anisotropic than the  $\text{TiO}_2$  II phase.

Alternatively and complementary, elastic anisotropy can be presented as the percentage difference in incompressibility and shear modulus computed by the Voigt and Reuss averages [45]:  $A_B = (B_V - B_R)/(B_V + B_R)$  and  $A_G = (G_V - G_R)/(G_V + G_R)$ . A value of zero indicates elastic isotropy and one is the maximum anisotropy. Using this formulation also allows a consideration of the monoclinic MI phase. As expected,  $A_B$  is smaller than  $A_G$  in all five forms of  $\text{TiO}_2$  (figure 2(B)).  $\text{TiO}_2$  II is least anisotropic, and rutile and the OII are most anisotropic (figure 2(B)), in agreement with the results from the Zener ratios (figure 2(A)).

## 5. Electronic structure

Figure 3 displays the densities of states (DOS) for the five phases at zero pressure. The electronic structure of  $\text{TiO}_2$  is

governed by a strong hybridization between the Ti 3d and the O 2p states around the Fermi level. It is very clear that  $\text{TiO}_2$  is a semiconductor with a small bandgap ( $\sim 2$  eV) in different forms. The upper valence band is dominated by oxygen 2p levels and its width increases from rutile to the OII phase. The lower valence band is at  $\sim 10$  eV smaller energy with a width of  $\sim 2.0\text{--}3.5$  eV, and is dominated by oxygen s levels. The lower conduction band is formed mainly by Ti 3d states. For rutile and  $\text{TiO}_2\text{II}$  there are two separate conduction bands below 8 eV, which are attributed to the crystal field splitting of the Ti 3d wavefunctions into states with  $t_{2g}$  and  $e_g$  symmetries in the  $\text{TiO}_6$  octahedral environment [46, 47]. However, a single and narrow conduction band appears in the MI, OI and OII phases, because an increase of the coordination number for Ti (MI: CN = 7; OI: CN = 7; and OII: CN = 9) makes Ti 3d electronic states more localized.

## 6. Conclusions

In the current work, we have investigated the structural stabilities, elastic properties, and electronic properties of five polymorphs of  $\text{TiO}_2$  observed experimentally, using the PAW-GGA and LAPW-GGA methods based on DFT. The computational results unambiguously demonstrate that the total energy of the  $\text{TiO}_2\text{II}$  is smaller than that of rutile at lower pressure, which can explain why the rutile phase is absent under decompression in experiments. The predicted phase transition sequence and transition pressures are consistent with experimental work [12, 13, 15, 16, 19, 20]. The bulk moduli have been analyzed and discussed based on equation of state fits and single crystal elastic constants: except for the soft MI phase,  $B_0$  for all phases falls in the range of 200–240 GPa, suggesting that the cotunnite (OII) phase is not a superhard material as has previously been claimed from experiments [17, 18] and some computations [27]. The electronic properties show that all five polymorphs of  $\text{TiO}_2$  considered here are semiconductors, and the lower conduction band is dominated by Ti 3d states that are sensitive to the coordination number of titanium.

## Acknowledgments

X Wu is grateful for his Alexander von Humboldt Fellowship and the financial support of the National Natural Science Foundation of China (Grant no. 40972029).

## References

- [1] Li J G, Ishigaki T and Sun D X 2007 *J. Phys. Chem. C* **111** 4969
- [2] Bach U, Lupo D, Comte P, Moser J E, Weissert F, Salbeck J, Spreitzer H and Gratzel M 1998 *Nature* **395** 583
- [3] Mattesini M, de Almeida J S, Dubrovinsky L, Dubrovinskaia N, Johansson B and Ahuja R 2004 *Phys. Rev. B* **70** 212101
- [4] Wu Y, Fei Y, Jin Z and Liu X 2009 *Earth Planet. Sci. Lett.* **282** 275
- [5] Navrotsky A, Jamieson J C and Kleppa O J 1967 *Science* **158** 388
- [6] Mitsuhashi T and Kleppa O J 1979 *J. Am. Ceram. Soc.* **62** 356
- [7] Ranade M R, Navrotsky A, Zhang H Z, Banfield J F, Elder S H, Zaban A, Borse P H, Kulkarni S K, Doran G S and Whitfield H J 2002 *Proc. Natl Acad. Sci. USA* **99** 485
- [8] Sheng P Y, Hwang S L, Chu H T, Yu T F, Pan C N and Huang W L 2005 *Eur. J. Mineral.* **17** 543
- [9] Simons P Y and Sharma M 1976 *Acta Crystallogr.* **23** 334
- [10] Sato H, Endo S, Sugiyama M, Kikagawa T, Shimomura O and Kusaba K 1991 *Science* **251** 786
- [11] Haines J and Leger J M 1993 *Physica B* **192** 233
- [12] Tang J and Endo S 1993 *J. Am. Ceram. Soc.* **76** 796
- [13] Gerward L and Olsen J S 1997 *J. Appl. Crystallogr.* **30** 259
- [14] Olsen J S, Gerward L and Jiang J Z 1999 *J. Phys. Chem. Solids* **60** 229
- [15] Arlt T, Bermejo M, Blanco M A, Gerward L, Jiang J Z, Olsen J S and Recio J M 2000 *Phys. Rev. B* **61** 14414
- [16] Dubrovinskaia N A, Dubrovinsky L S, Ahuja R, Prakapenka V B, Dmitriev V, Weber H P, Osorio-Guillen J M and Johansson B 2001 *Phys. Rev. Lett.* **87** 275501
- [17] Dubrovinsky L, Dubrovinskaia N, Swamy V, Muscat J, Harrison N M, Ahuja R, Holm B and Johansson B 2001 *Nature* **410** 653
- [18] Ahuja R and Dubrovinsky L 2002 *J. Phys.: Condens. Matter* **14** 10995
- [19] Nishio-Hamane D, Shimizu A, Nakahira R, Niwa K, Sano-Furukawa A, Okada T, Yagi T and Kikegawa T 2010 *Phys. Chem. Miner.* **37** 129
- [20] Al-Khatatbeh Y, Lee K K M and Kiefer B 2009 *Phys. Rev. B* **79** 134114
- [21] Swamy V and Muddle B C 2007 *Phys. Rev. Lett.* **98** 035502
- [22] Liang Y, Zhang B and Zhao J 2008 *Phys. Rev. B* **77** 094126
- [23] Mammone J F and Sharma M 1980 *Solid State Commun.* **34** 799
- [24] Arashi H 1992 *J. Phys. Chem. Solids* **53** 355
- [25] Liu L and Mernagh T P 1992 *Eur. J. Mineral.* **4** 45
- [26] Dewhurst J K and Lowther J E 1996 *Phys. Rev. B* **54** R3673
- [27] Muscat J, Swamy V and Harrison N M 2002 *Phys. Rev. B* **65** 224112
- [28] Sasaki T 2002 *J. Phys.: Condens. Matter* **14** 10557
- [29] Caravaca M A, Miño J C, Pérez V J, Casali R A and Ponce C A 2008 *J. Phys.: Condens. Matter* **21** 015501
- [30] Kočí L, Kim D Y, De Almeida J S, Mattesini M, Isaev E and Ahuja R 2008 *J. Phys.: Condens. Matter* **20** 345218
- [31] Kresse G and Furthmüller J 1996 *Phys. Rev. B* **54** 11169
- [32] Blaha P, Schwarz K, Madsen G K H, Kvasnicka D and Luitz J 2002 *WIEN2k, An Augmented Plane Wave Local Orbitals Program for Calculating Crystal Properties*, revised edition June 2002, Univ Prof. Dr. Karlheinz Schwarz, Technische Universität Wien, Institut für Physikalische und Theoretische Chemie, Getreidemarkt 9/156A-1060Wien/Austria
- [33] Kresse G and Joubert D 1999 *Phys. Rev. B* **59** 1758
- [34] Perdew J P, Burke K and Ernzerhof M 1996 *Phys. Rev. Lett.* **77** 3865
- [35] Birch F 1947 *Phys. Rev.* **71** 809
- [36] Mookherjee M and Steinle-Neumann G 2009 *Geophys. Res. Lett.* **36** L08307
- [37] Iuga M, Steinle-Neumann G and Meinhardt J 2007 *Eur. Phys. J. B* **58** 127
- [38] Ming L C and Manghani M H 1979 *J. Geophys. Res.* **84** 4777
- [39] Isaak D G, Carnes J D, Anderson O L, Cynn H and Hake E 1998 *Phys. Chem. Miner.* **26** 31
- [40] Grimsditch M H and Ramdas A K 1976 *Phys. Rev. B* **14** 1670
- [41] Manghnani M H 1969 *J. Geophys. Res.* **74** 4317
- [42] Hill R 1952 *Proc. Phys. Soc., Lond. A* **65** 349
- [43] Watt J P 1987 *Comput. Geosci.* **13** 441
- [44] Zener C 1948 *Elasticity and Anelasticity of Metals* (Chicago, IL: University of Chicago Press) p 16
- [45] Panda K B and Chandran K S R 2006 *Acta Mater.* **54** 1641
- [46] Mo S D and Ching W Y 1995 *Phys. Rev. B* **51** 13023
- [47] Stoyanov E, Langenhorst F and Steinle-Neumann G 2007 *Am. Mineral.* **92** 577